

A Theoretical Assessment of the Relative Performance of Spherical Phased Arrays for Ultrasound Surgery

Leonid R. Gavrilov¹ and Jeffrey W. Hand

Abstract—Computer modeling of spherical-section phased arrays for ultrasound surgery (tissue ablation) is described. The influence on performance of the number of circular elements (64 to 1024), their diameter (2.5 to 10 mm), frequency (1 to 2 MHz), and degree of sparseness in the array is investigated for elements distributed randomly or in square, annular, and hexagonal patterns on a spherical shell (radius of curvature, 120 mm). Criteria for evaluating the quality of the intensity distributions obtained when focusing the arrays both on and away from their center of curvature, and in both single focus and simultaneous multiple foci modes, are proposed. Of the arrays studied, the most favorable performance, for both modes, is predicted for 256 5-mm diameter, randomly distributed elements. For the single focus mode, this performed better than regular arrays of 255 to 1024 elements and, for the case of nine simultaneous foci produced on a coplanar 3×3 grid with 4-mm spacing, better than square, hexagonal, or annular distributed arrays with a comparable number of elements. Randomization improved performance by suppressing grating lobes significantly. For single focus mode, a several-fold decrease in the number of elements could be made without degrading the quality of the intensity distribution.

I. INTRODUCTION

THERE is interest in developing minimally invasive therapeutic ultrasound techniques for surgery (tissue ablation) because these may offer potential benefits compared with conventional approaches in terms of reduced morbidity, increased patient acceptability, and reduced in-patient time. Much of the work previously reported has involved the use of a single or a few piezoceramic transducers with spherical curved surfaces [1]–[4], phased arrays with various sizes and operating regimes [5]–[11], and lenses [12]–[15].

Although systems based on the use of a single-focused transducer have the advantage of being relatively simple, they have disadvantages, including the need to scan the focus by mechanically translating the transducer to treat clinically relevant volumes of tissue. In addition to the production of lesions, the level of tissue heating in regions proximal to the focal plane and the duration of treatment are important aspects of ultrasound surgery. These are dependent on the ultrasound intensity, the duration of the

ultrasound pulses, the temporal delay between them, and the spatial separation between neighboring targets. The latter two factors may be excessive when a single focus is scanned [5]–[8].

Some of these challenges may be met by using phased arrays that offer electronically controlled dynamic focusing and the ability to vary and control precisely the range, location and size of the focus during treatment without moving the array [5]–[11], [16]–[20]. Several investigators have proposed the use of phased arrays in which elements are placed on a spherical shell, thereby combining electronic and geometric focusing. Because phased arrays also offer means of synthesizing fields with multiple simultaneous foci, their use is expected to reduce the time taken to deliver ablative therapy [5]–[11].

Disadvantages of phased arrays include the unwanted presence of grating lobes and other secondary intensity maxima and, particularly for relatively large extracorporeal, 2-D arrays, complexity and potentially relatively high cost. The need to reduce grating lobes is common to all therapeutic arrays reported to date, and several techniques aimed at achieving this have been reported. A random distribution of different-sized elements in a linear phased array has been investigated [19], [20]; grating lobe levels associated with an aperiodic distribution of elements were approximately 30 to 45% less than those associated with periodic center-to-center element spacing. Goss *et al.* [11] showed theoretically that the use of elements randomly distributed on a segment of a spherical surface may improve phased array performance. Those researchers also suggested that the use of sparse phased arrays may be promising in the reduction of the complexity and relatively high cost of large 2-D arrays. Apodization, broad banding, and the use of subsets of elements have also been investigated [21]–[23]. In work related to phased arrays for imaging, differing periodic spacings for transmit and receive elements have been used [24], [25], resulting in the transmit and receive grating lobes occurring at different locations where their contribution to the two-way radiation pattern cancel.

In the present work, computer modeling and analysis of the performance of several sparse, quasi-random, ultrasound phased arrays mounted on a segment of a spherical surface and intended for ablation are described, and the results are compared with those obtained for periodic arrays.

Manuscript received March 2, 1999; accepted October 4, 1999.

L. R. Gavrilov and J. W. Hand are with the Radiological Sciences Unit, Department of Imaging, Hammersmith Hospital, London W12 0HS, U.K. (e-mail: j.hand@ic.ac.uk).

¹Current address: Acoustics Institute, Moscow, 117036, Russia.

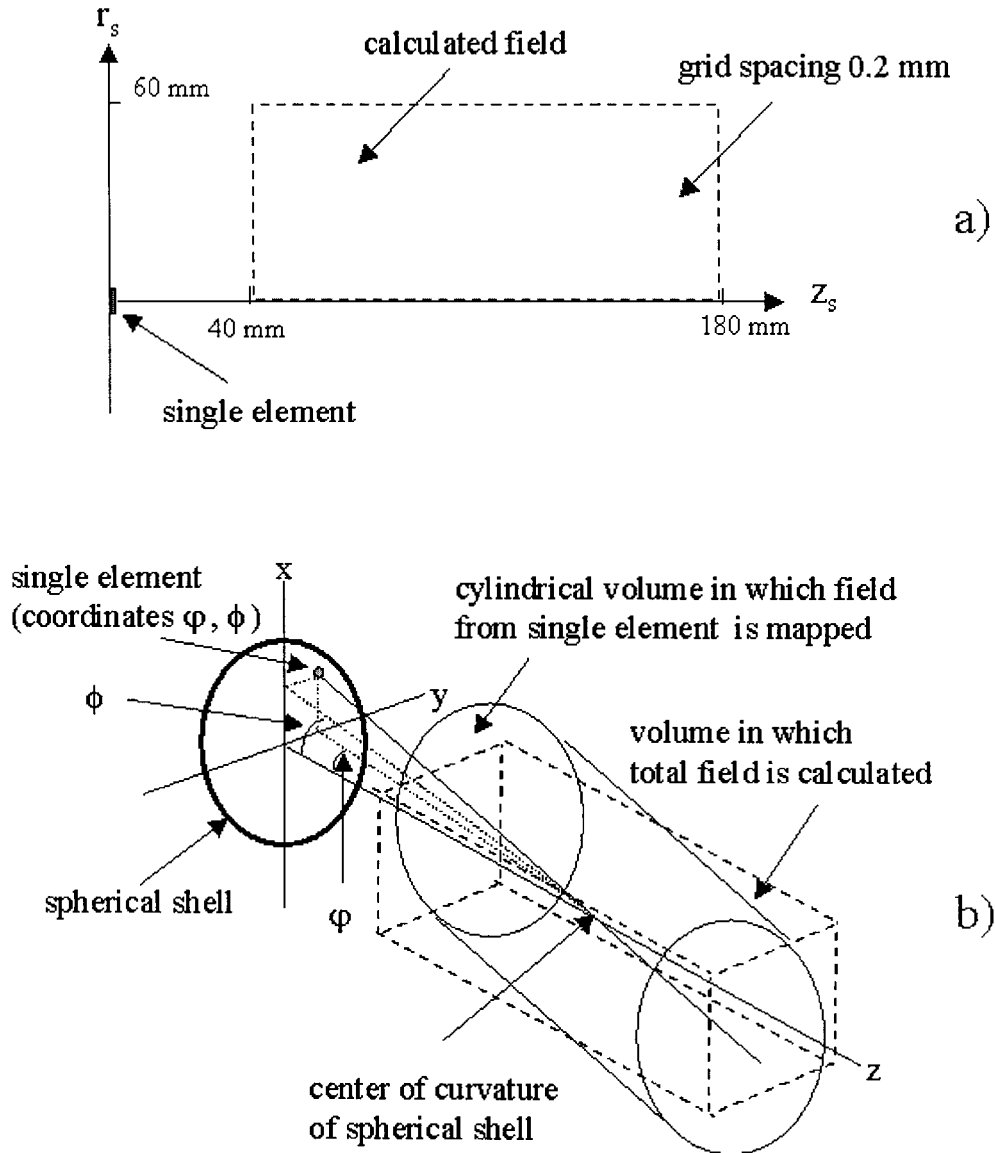


Fig. 1. Schematic illustration of the method used for calculations: a) calculated field of a single element and b) calculated field of an array.

II. METHODS

The intensity distributions were calculated in a manner essentially similar to that described in [11]. Fig. 1 is a schematic illustration of the method used. The complex pressure distribution associated with a single plane circular element was found using the Point Radiator Method (or the Point Source Method) in which the acoustic piston source is represented by many point radiators [26]. Square elemental radiators of side length 0.25 mm were used to describe the radiating surface of each circular element. Assuming radial symmetry for a circular element, its 3-D acoustic field was found [11] by calculating the complex pressure $p(r_s, z_s)$ as a function of axial distance from the element, z_s , and distance off its central axis, r_s according to

$$p(r_s, z_s) = \frac{j\rho ck u_0 \Delta A}{2\pi} \sum_{\text{surface}} \frac{e^{-(\alpha + jk)R}}{R}$$

where ρ is the tissue density ($1000 \text{ kg}\cdot\text{m}^{-3}$), c is speed of sound in the tissue ($1500 \text{ m}\cdot\text{s}^{-1}$), k is the propagation constant, u_0 is the velocity amplitude of the surface of the elemental sources, ΔA is the area of each elemental source, α is the attenuation coefficient in the tissue, and R is the distance from the center of an elemental source to the point (r_s, z_s) where the field is calculated. In general, calculations were carried out for $40 \leq z_s \leq 180 \text{ mm}$ and $0 \leq r_s \leq 60 \text{ mm}$, both in spatial increments of 0.2 mm (Fig. 1a). The attenuation coefficient in the tissue α was taken to be $10 \text{ Np}\cdot\text{m}^{-1} \text{ MHz}^{-1}$, which, although toward the high end of the range found in the literature, is a value used previously by many researchers for similar calculations [6], [17], [19], [20], [27].

The total complex pressure distributions from various arrays of plane circular elements mounted on a spherical shell (radius of curvature = 120 mm in all cases) were calculated by summing the complex pressure contributions

TABLE I
LOCATIONS AND RELATIVE PHASE VALUES FOR THE NINE COPLANAR
FOCI.

$x + 4, y - 4, z$	$x + 4, y, z$	$x + 4, y + 4, z$
•	•	•
0	$\pi/4$	$\pi/2$
$0, y - 4, z$	$0, y, z$	$0, y + 4, z$
•	•	•
$7\pi/4$	$\pi/2$	$3\pi/4$
$x - 4, y - 4, z$	$x - 4, y, z$	$x - y + 4, z$
•	•	•
$3\pi/2$	$5\pi/4$	π

from each element in an array at each point in the 3-D volume of interest (Fig. 1b). Knowing the complex pressure as a function of axial and radial distances for the single element whose center was defined by the angular coordinates ϕ and φ (the angles subtended at the center of curvature in the vertical and horizontal planes, respectively), the values were mapped from the rotated cylindrical volume to points on a 0.2-mm, 3-D rectangular grid aligned with the Cartesian axes. Calculations were carried out over the volume defined by $50 \leq z \leq 160$ mm axially and $-30 \leq x$ and $y \leq 30$ mm (in a few cases to ± 40 mm to ensure inclusion of grating lobes).

The relative phases of the surface velocity at each circular element required to produce a single focus were determined from the paths between the centers of each element and the position of the focus. To produce simultaneous multiple foci, the complex surface velocity u_n at the n^{th} of the N circular elements was determined using the method first described by Ebbini and Cain [17]. The u_n are related to the complex pressures p_m at each of M target or control points, by the matrix equation

$$\mathbf{u} = \mathbf{H}^{*t} (\mathbf{H}\mathbf{H}^{*t})^{-1} \mathbf{p}$$

where $\mathbf{u} = [u_1, u_2, \dots, u_n, \dots, u_N]^t$, $\mathbf{p} = [p_1, p_2, \dots, p_m, \dots, p_M]^t$, and \mathbf{H} is the $M \times N$ matrix. We used elements $h_{mn} = \frac{\exp(-jk r_{mn})}{r_{mn}}$ where r_{mn} is the distance from the m^{th} target point to the center of the n^{th} element. \mathbf{H}^{*t} is the conjugate transpose of \mathbf{H} and $[\]^t$ denotes transpose. In this study, the set of M target points was selected to be within the same focal plane and to lie on a uniformly spaced $\sqrt{M} \times \sqrt{M}$ grid. To determine the $u_n (n = 1, 2, \dots, N)$, the phases and amplitudes of the $p_m (m = 1, 2, \dots, M)$ must be selected. We chose equal amplitudes and imposed a rotation of phase around the pattern of foci in a manner similar to that used in [9] and shown for the case of a 3×3 pattern with 4-mm spacing in Table I. Here, co-ordinates (upper figures) are referenced to the central focus at the point $(0, y, z)$ and shifts are in millimeters. The relative phases of the complex pressure at these nine locations are shown by the lower figures.

The intensity at each grid point was found from the product of the complex pressure and its complex conjugate, and the distribution was normalized with respect to

the global maximum intensity obtained within the volume of interest.

Calculations of the pressure and intensity field distributions were carried out using 1) a Silicon Graphics Onyx2 computer with programs written in FORTRAN 77 and 2) a Pentium II based PC with programs written in Microsoft Fortran PowerStation 4.0 based on Fortran 90. The data were analyzed using AVS v5 (Advanced Visual Systems Inc., Waltham, MA) and Matlab v5.2.1 (Mathworks Inc., Natick, MA) running on the Onyx2 and Axum v5.0 (MathSoft Inc., Cambridge, MA) running on the PC. Three-dimensional intensity distributions were analyzed qualitatively and data in selected planes were analyzed quantitatively.

The 2-D intensity distributions presented in this work represent in the main data in the y - z plane. This plane contained the ultrasound focus when it was not coincident with the center of curvature and was a worst case in terms of the level of grating lobes. In some cases (see subsequently), calculations were also carried out with the focus located in the x - z plane.

The influence on array performance of several parameters, such as the number of elements (64, 128, 255, 256, and 1024), their diameter (2.5, 5, 7, and 10 mm), frequency (1, 1.5, and 2 MHz), and level of sparseness, was investigated. Calculations were made for arrays with elements distributed randomly on the shell (Fig. 2) as well as for arrays with elements distributed regularly on the shell in square, annular, and hexagonal patterns (Fig. 3). The diameters of all the arrays presented in Fig. 2 and 3, which show the locations but not the dimensions of the elements, were equal to 110 mm.

The first array consisted of 256 elements, each 5 mm in diameter, distributed in a quasi-random manner (a completely random distribution was modified such that the minimum separation between centers of elements was 5.5 mm) and is shown schematically in Fig. 2(a). Three driving frequencies were considered –1, 1.5, and 2 MHz. Several similar quasi-random distributions of elements on the shell were investigated, but the differences in results were negligible. Calculations were also made for quasi-randomly distributed arrays of 128 elements, each 7 mm in diameter [Fig. 2(b)], and of 64 elements, each 10 mm in diameter [Fig. 2(c)]. The frequency in both of these cases was 1.5 MHz, and the minimum separation between centers of elements was 7.5 and 10.5 mm, respectively.

Fig. 3 illustrates some regular arrays investigated in this work; all were assumed to operate at 1.5 MHz. Fig. 3(a) is a schematic representation of an array of 256 elements, each 5 mm in diameter, placed on the shell in a square configuration. The minimum separation between centers was 5.5 mm. Fig. 3(b) shows a similar array of 1024 elements, each 2.5 mm in diameter; in this case, the center-to-center spacing was 2.75 mm. Fig. 3(c) shows an annular array of 255 elements, each 5 mm in diameter, consisting of a central element and nine concentric rings with radii increasing from 5.5 to 49.5 mm in multiples of 5.5 mm. The rings contain 5, 11, 17, 23, 28, 33, 40, 46, and 51 elements, re-

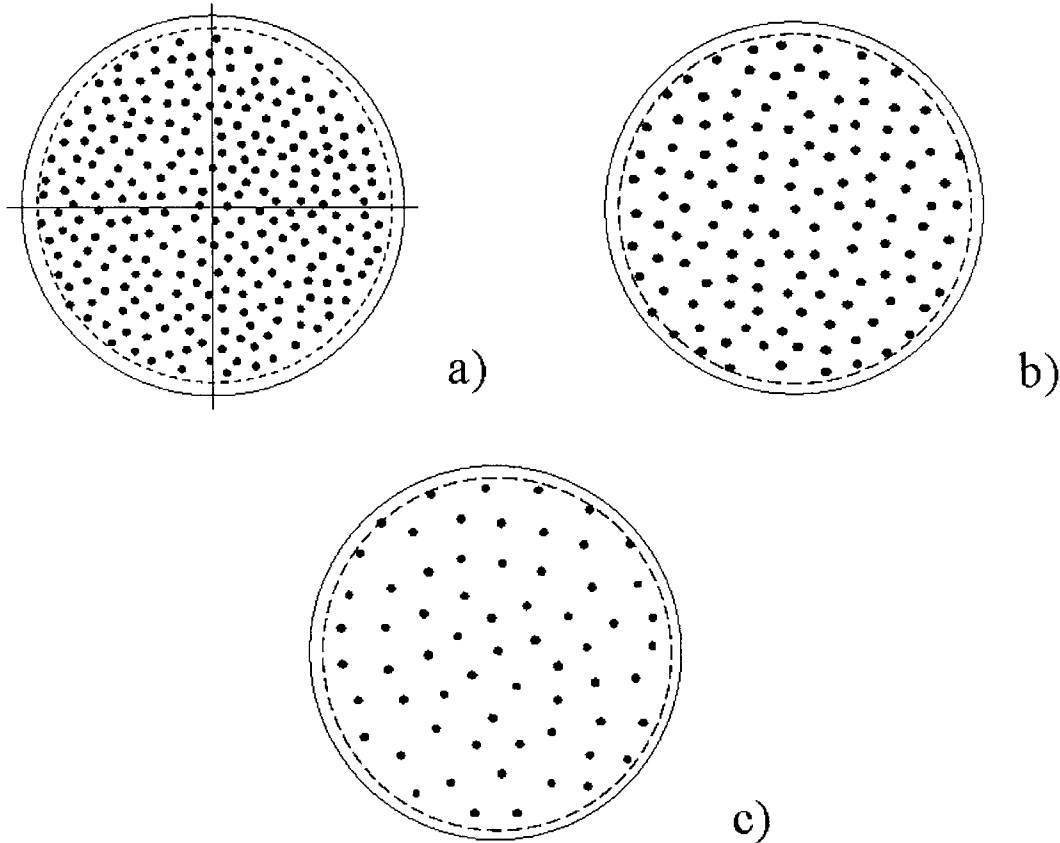


Fig. 2. Schematic drawings of arrays with plane circular elements distributed on the spherical shell in a quasi-random manner: a) 256 elements, each 5 mm in diameter; b) 128 elements, each 7 mm in diameter; and c) 64 elements, each 10 mm in diameter. The minimum center-to-center distance between elements is 5.5, 7.5, and 10.5 mm, respectively. The diameter of all arrays is 110 mm, and the maximum center-to-center distance between elements is 100 mm.

spectively, with center-to-center spacing of 6 mm. Fig. 3(d) shows an array consisting of 255 elements, each 5 mm in diameter, placed in a hexagonal configuration with center-to-center spacing of 5.5 mm. The arrays presented in Fig. 2 and 3 have approximately the same (within 1.5%) active area of 50 cm^2 and so, in theory, should be able to provide approximately the same acoustic power.

Four criteria were selected to assess the quality of the normalized intensity distributions calculated for these arrays used in the single focus mode. First, an intensity distribution was deemed to be grade A when intensity $I \geq 0.1 I_{\max}$ occurred only within the focal region and was absent in the remainder of the plane investigated. This criterion is in agreement with the commonly expressed opinion that the maximum intensity in grating lobes should be at least 8 to 10 dB lower than that in the main lobe for safe delivery of treatment [11], [17], [19]. The intensity distribution was described as grade B when there were < 10 localized areas in which the intensity was in the range $0.1 \leq I \leq 0.15 I_{\max}$ outside the focal area in the plane considered. Intensity distributions with > 10 localized areas outside the focal area in the plane considered in which $0.1 \leq I < 0.15 I_{\max}$ were classified grade C. Finally, further discrimination among poor intensity distributions was provided by a grade D classification for those where there was at least one localized area in which $I \geq 0.2 I_{\max}$.

Because, in practice, the treatment volume will be larger than that associated with a single focus, multiple lesions will be needed and achieved by electronically scanning the location of the single focus, by synthesizing simultaneously a pattern of multiple foci, or by scanning a small pattern of simultaneous multiple foci [6]–[9]. In all of these cases, the pre-focal intensity (or time-averaged intensity) will be considerably greater than that associated with grades A through D described previously. Correspondingly, possible criteria for evaluation of quality of intensity distributions associated with multiple foci will be less rigorous than those for the single focus mode.

Fan and Hynynen [6] reported that elevations of tissue temperature to 53.5°C for 10 s and 56.8°C for 1 s each result in the same thermal dose that is a threshold value for tissue necrosis. The maximum temperature T_{\max} achieved during ultrasound surgery is often in the range of 80 to 90°C [3], [6], [9]. Thus, in terms of temperature increase ΔT (with respect to 37°C), tissue necrosis is likely to be achieved over the approximate range of 0.4 to $1.0 \Delta T_{\max}$ where ΔT_{\max} is the maximum increase in temperature produced. If the effects of thermal conduction and perfusion are neglected during relatively brief exposures of a few seconds, and ΔT and intensity I are assumed to be linearly related, then to a first-order approximation, a basis of classifying pre-focal intensity levels and intensity hot spots in

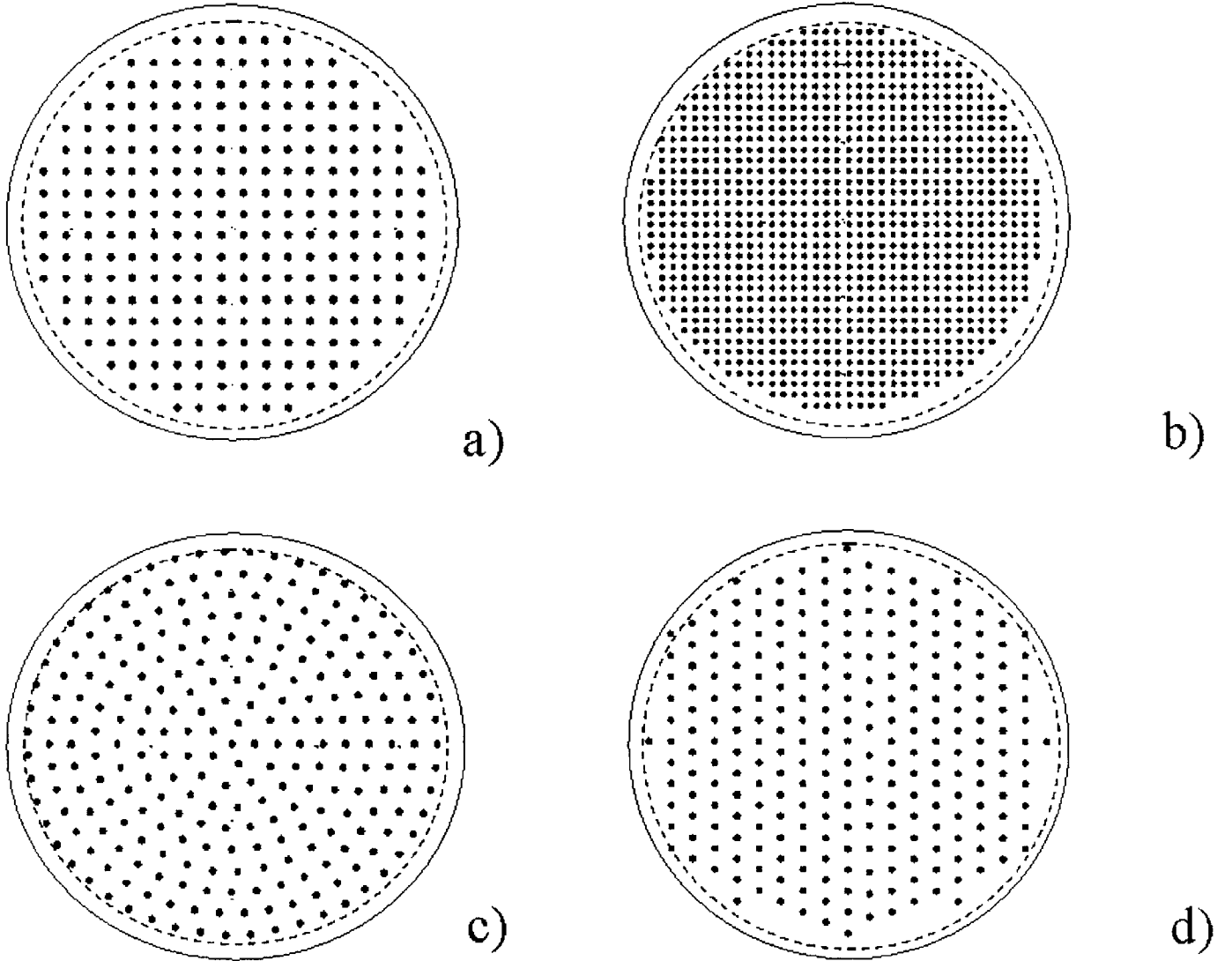


Fig. 3. Schematic drawing of arrays with circular elements distributed on the spherical shell in regular patterns: a) 256 elements, each 5 mm in diameter and distributed in a square pattern; b) 1024 elements, each 2.5 mm in diameter and distributed in a square pattern; c) 255 elements, each 5 mm in diameter and distributed in an annular pattern; and d) 255 elements, each 5 mm in diameter and distributed in a hexagonal pattern. The diameter of all arrays is 110 mm, and the maximum center-to-center distance between elements is 100 mm.

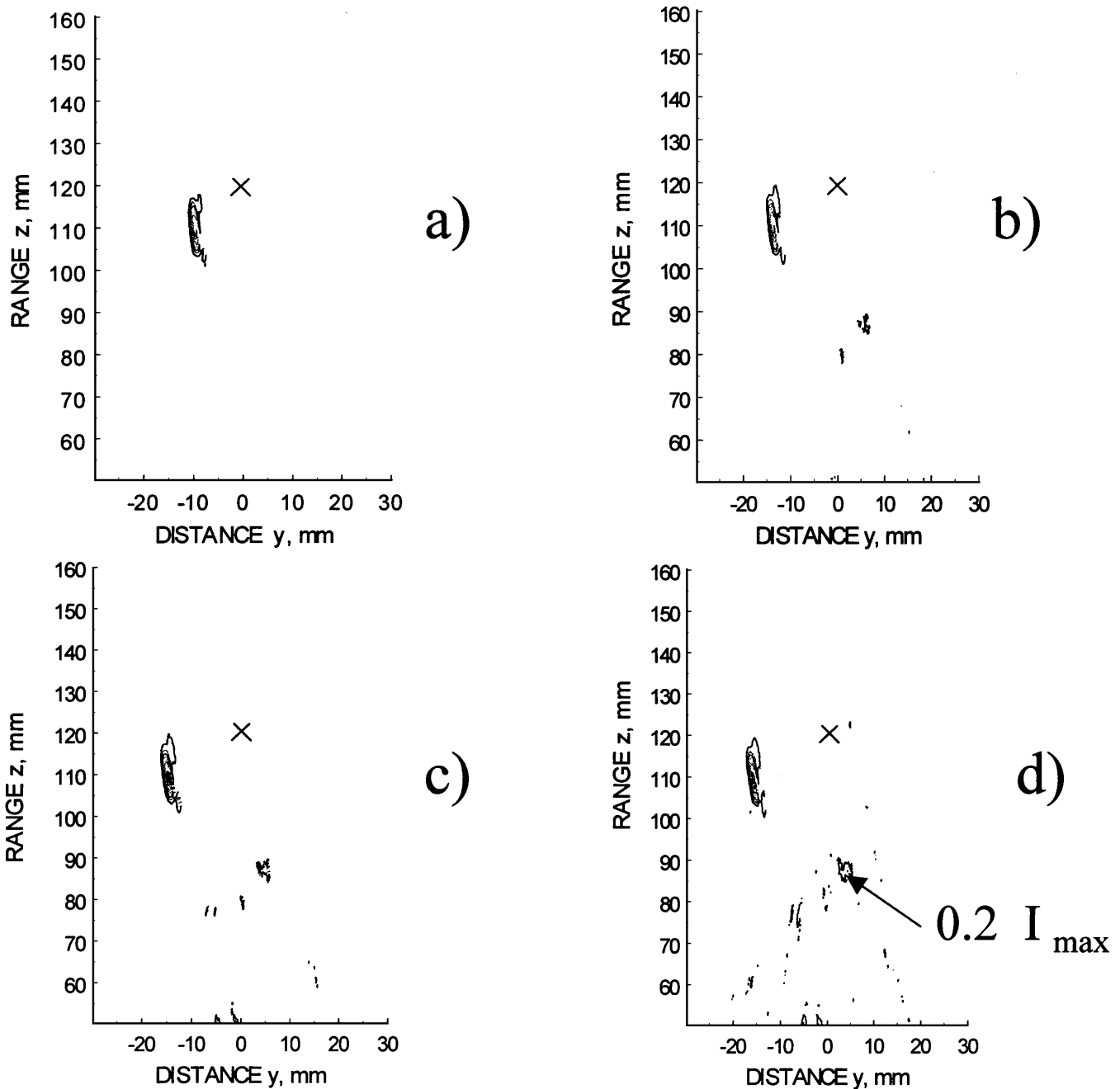
distributions associated with multiple foci might be as follows. Grade I: $I \leq 30\% I_{\max}$ outside the multiple foci pattern, grade II: $30\% I_{\max} < I \leq 40\% I_{\max}$ outside the multiple foci pattern, and grade III: $I > 40\% I_{\max}$ outside the multiple foci pattern. The risks of producing thermal necrosis outside of the target area should be low for grade I and significant for grade III. These grades may be conservative because no account of cooling between ultrasound pulses is considered.

III. RESULTS

Fig. 4(a and b) shows examples of intensity distributions for the random array of 256 5-mm elements [see Fig. 2(a)] driven at a frequency of 1.5 MHz in the single focus mode. This figure illustrates the dependence of quality of the intensity distribution on the location of the focus. Displacement of the focus from 10 to 16 mm off the acoustical axis (at a range of 110 mm) changes the quality

from grade A to grade D. In Fig. 4(a), nine contours (10 to 90% I_{\max} in increments of 10% I_{\max}) are drawn inside the focal region. The intensity distribution in the remainder of the plane outside the focal region was assessed in terms of contours at 10 to 20% I_{\max} in increments of 5% I_{\max} and, in a few cases, by contours at 10 to 20% I_{\max} in increments of 2% I_{\max} . Characterization of the intensity distributions associated with this array driven at 1, 1.5, and 2 MHz is summarized in Fig. 5. Fig. 5 presents data for displacements of the focus in the positive y-direction (as do Fig. 6 through 8). Calculations were also carried out for foci displaced in the negative y-direction, and the results were qualitatively very similar. Quantitative differences in intensity distributions were typically very small.

Fig. 6(a) illustrates the effect of increasing the sparseness in a random array of 5-mm diameter elements. The characterization of the intensity distribution shown is for the case when one-half of 256 randomly distributed ele-



ments were selected at random to be switched off. The driving frequency was 1.5 MHz.

Assessments of the intensity distributions for the 1.5-MHz random arrays of 128 7-mm diameter elements [see Fig. 2(b)] and 64 10-mm diameter elements [see Fig. 2(c)] are shown in Fig. 6(b and c), respectively. Data shown in Fig. 5 and 6 were based on calculations carried out with the focus located in the y - z plane. Calculations in the x - z plane (not shown here) yielded qualitatively very similar results.

The results of assessing intensity distributions for 1.5 MHz, regular-spaced arrays [see Fig. 3(a through d)] are shown in Fig. 7 and 8. For the regular arrays with square and annular patterns, calculations were carried out with the focus located in the y - z plane (Fig. 7). Calcu-

lations were also made in the x - z plane (not presented) and yielded qualitatively very similar results. The hexagonal regular array had different performance in y - z and x - z planes, and both are shown in Fig. 8.

As a preliminary assessment of the relative performance of some of the arrays when used in a simultaneous multiple foci mode, intensity patterns associated with the production of nine foci, located in a focal plane and at points defined by a 3×3 matrix with 4-mm separation between foci were considered. In all cases, the relative phase rotation between the nine targeted locations shown in Table I was adopted.

Fig. 9 shows examples of intensity distributions associated with this multiple foci pattern and produced by the 256 5-mm element random array driven at 1.5 MHz. In

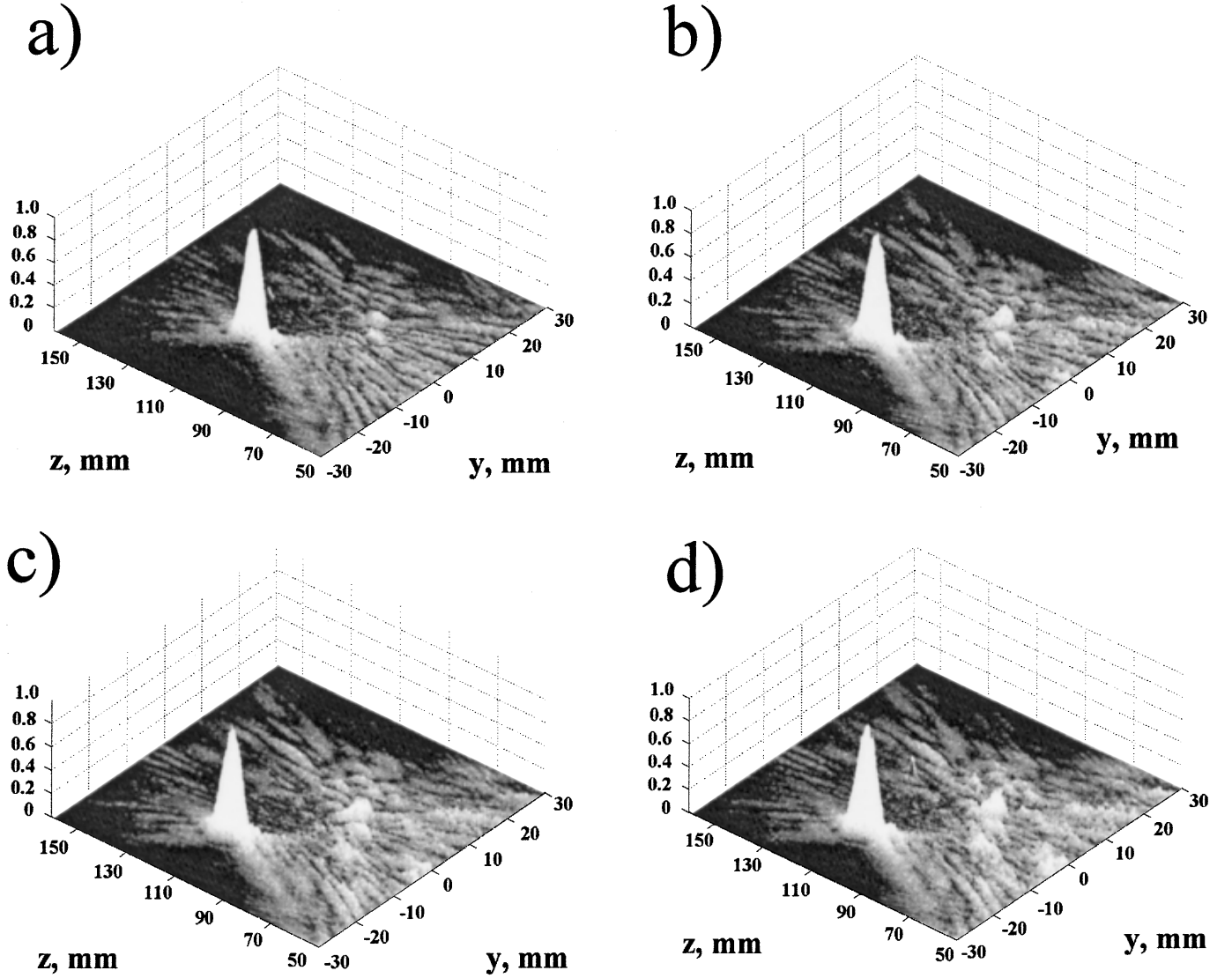


Fig. 4. A) (previous page) Examples of the intensity field distributions for the single focus mode and criteria used for estimating the quality of the intensity distributions: a) A grade, b) B grade, c) C grade, and d) D grade. The symbol “x” corresponds to the location of the center of curvature. These examples are for a random array of 256 5-mm diameter circular elements [Fig. 2(a)] driven at 1.5 MHz. The focus is located at a) 0, -10, and 110 mm b) 0, -14, and 110 mm; c) 0, -15, and 110 mm; and d) 0, -16, and 110 mm. B) Intensity distributions for the same cases as in Fig. 4(A) but with $0 \leq I \leq 0.1 I_{\max}$ depicted by a linear gray scale and $I > 0.1 I_{\max}$ shown in white.

each case, the central focus in the pattern was located on the central axis but, from left to right, at a range of 100, 110, and 120 mm. The resulting intensity distributions correspond to grades I, II, and III, respectively.

Fig. 10 summarizes the characteristics of intensity distributions associated with four 1.5-MHz arrays when the co-ordinates of the central focus in the 3×3 coplanar pattern are varied over the ranges of z and y shown. Fig. 10(a, b, c, and d) shows data obtained for 256 5-mm randomly distributed elements, 256 5-mm elements in a square pattern, 255 5-mm elements in a hexagonal pattern, and 255 5-mm elements in the annular configuration.

Fig. 11 shows intensity distributions in the x - y plane for the four arrays referred to in Fig. 10 when the 3×3 pattern is produced at a range of 100 mm. The patterns relate to 1) elements in the random pattern, 2) elements in

the square pattern, 3) elements in the hexagonal pattern, and 4) elements in the annular pattern. For all arrays, the upper graphs show the central focus in the pattern steered to the point $x = 0$, $y = 0$, and $z = 100$ mm; the lower ones show the case when it is steered to the point $x = 0$, $y = 10$, $z = 100$ mm.

IV. DISCUSSION

We have assessed the quality of the intensity distributions produced by phased arrays for both single focus and multiple foci modes by considering values of the intensity in grating lobes and other intensity maxima in the plane containing the focus (or central focus of coplanar, square, multiple foci patterns) for both random and regular arrays and within an area of 110 mm (in range) by 60 mm (laterally). In the single focus mode, the array consisting of

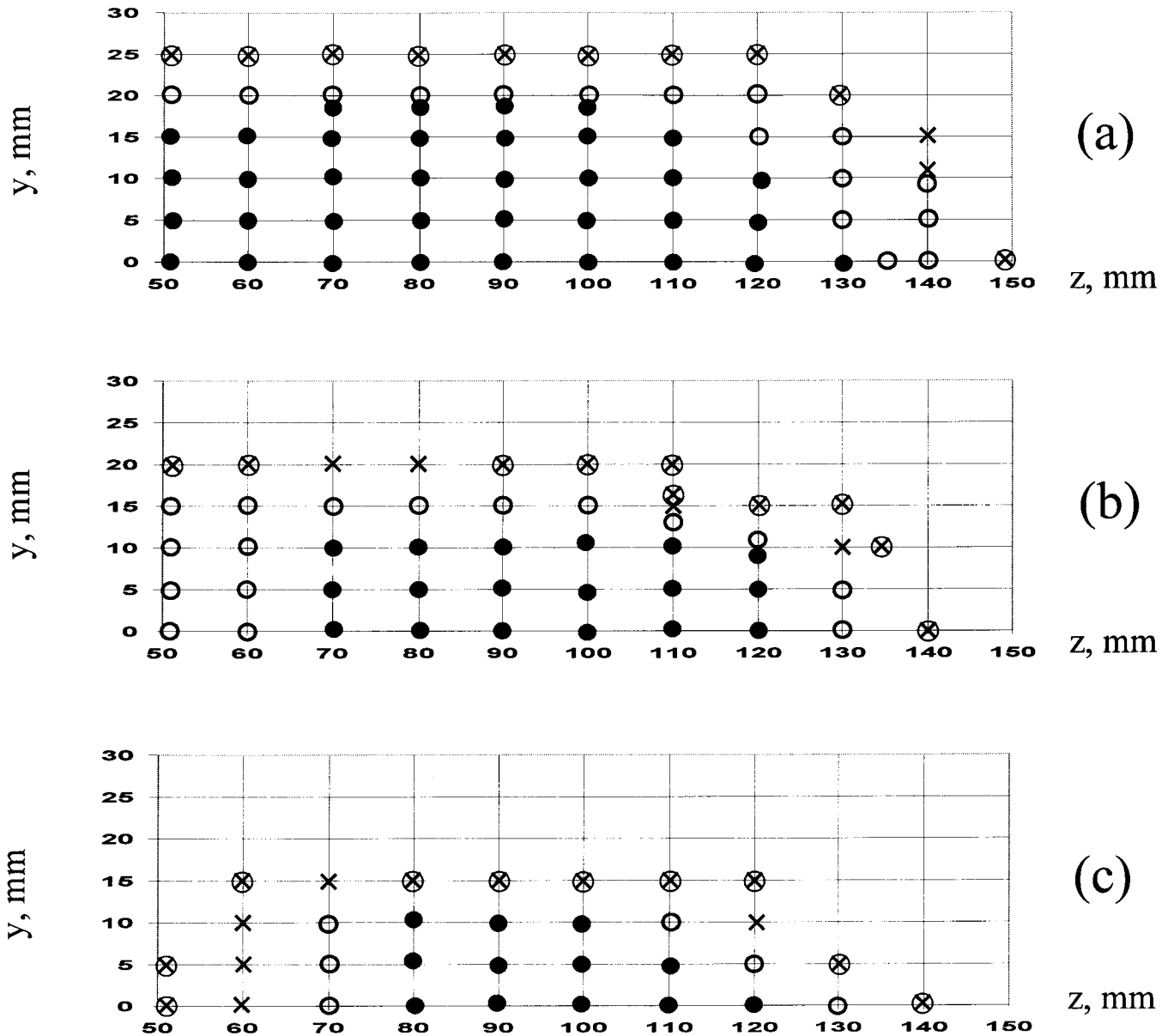


Fig. 5. Summary of results of calculations and quality assessment of the intensity distributions for the single focus mode associated with the random array of 256 5-mm diameter elements [Fig. 2(a)]. Frequencies: a) 1 MHz, b) 1.5 MHz, and c) 2 MHz. The quality levels are: A grade (●), B grade (○), C grade (×), and D grade (⊗).

256 plane circular elements, each 5 mm in diameter, distributed in a quasi-random manner and driven at 1 MHz could steer the focus up to ± 20 mm off center over ranges from 50 to 120 to 140 mm and still achieve a good quality rating (grades A or B) [see Fig. 5(a)]. At 1.5 MHz, the distances over which the focus could be steered compatible with A and B ratings were ± 10 mm for ranges within 70 to 120 mm and ± 15 mm for ranges from 50 to 120 mm, respectively [Fig. 5(b)]. The grade A criterion used here for the single focus mode was more rigorous than using the ratio between the maximum intensity in the grating lobes in the focal plane only and that in the focus, as used in [11].

The performance of the array as assessed by the quality of the intensity distribution is dependent on both the dis-

tance of the focus from the center of curvature and attenuation. Fig. 5 shows that when the focus is steered beyond the shell's center of curvature, the quality of the intensity distribution decreased abruptly. It is observed also that the greatest steering of the focus off center with a grade A quality may be achieved at a range approximately 1 to 2 cm proximal to the center of curvature. The volume over which a grade A (or B) intensity is maintained varies from 63 (or 106) cm^3 at 1 MHz [Fig. 5(a)], through 16 (or 49) cm^3 at 1.5 MHz [Fig. 5(b)], to 12.5 (or 16) cm^3 at 2 MHz [Fig. 5(c)], respectively.

In the array consisting of 256 5-mm diameter elements, the ratio of the total area of elements (active area) to the area of the shell was approximately 51%. A significant deterioration of the array's performance occurred when the

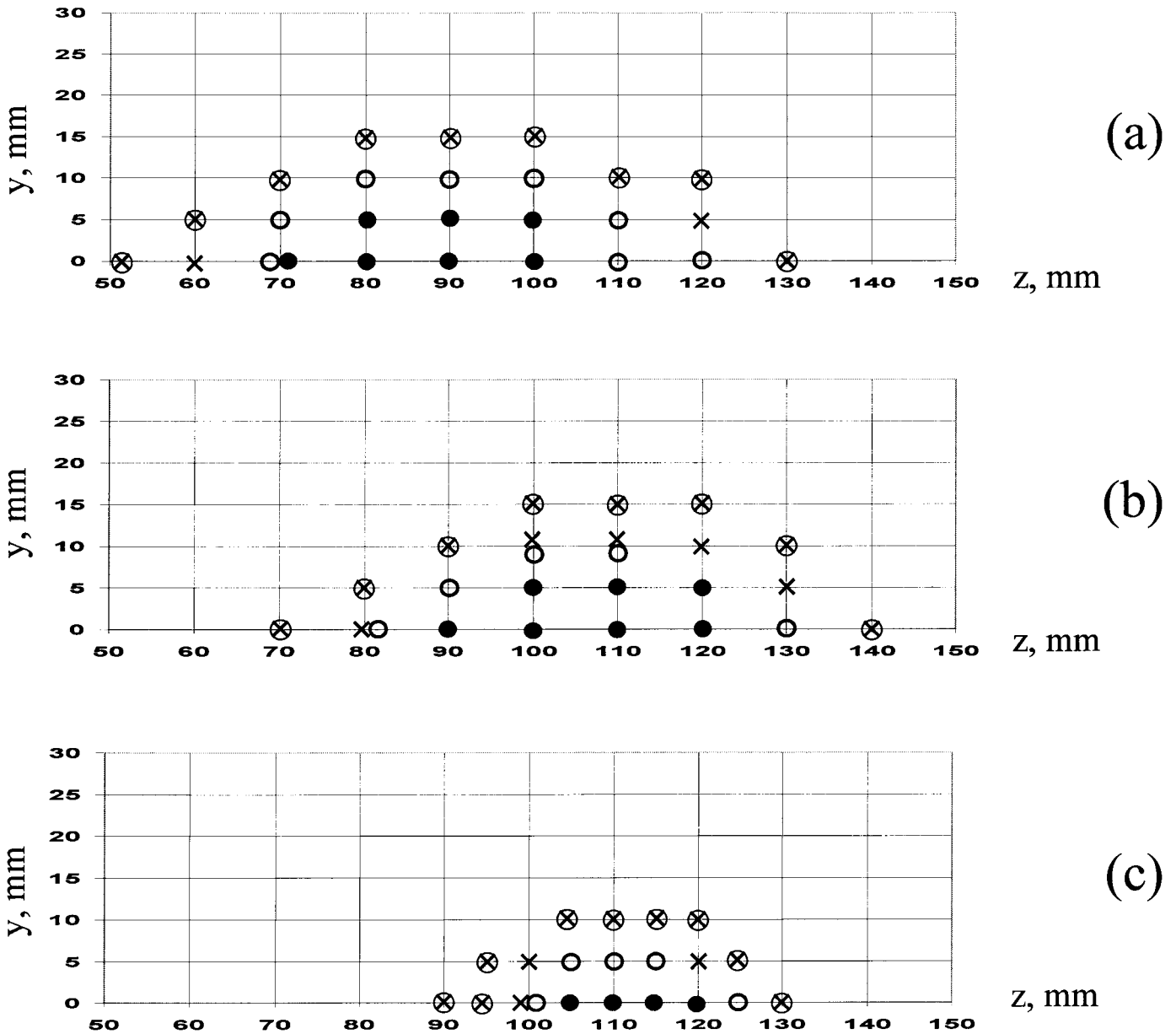


Fig. 6. Assessment of the quality of intensity distributions for the single focus mode associated with a) the random array consisting of 128 elements, randomly selected from the 256×5 -mm elements array shown in Fig. 2(a); b) the array of 128×7 mm randomly distributed circular elements [Fig. 2(b)]; and c) the array of 64×10 mm randomly distributed circular elements [Fig. 2(c)]. The frequency is 1.5 MHz. The quality levels are A grade (●), B grade (○), C grade (×), and D grade (⊗).

sparseness of the array was increased (one-half of the 256 elements were switched off at random) [Fig. 6(a)]. In this case, not only did the useful treatment volume become much smaller, but the greatest range at which the focus could be located compatible with an A-graded intensity distribution rating was reduced to 100 mm.

Decreasing the number of randomly distributed elements from 256 through 128 to 64, while simultaneously increasing the diameter of the elements (from 5 through 7 to 10 mm, respectively) to maintain a constant active area also led to progressive deterioration of the array’s performance [Fig. 6(b and c)]. The differences in the qualities of intensity distributions associated with the array of 128 elements, each 5 mm in diameter, and that of 128 elements,

each 7 mm in diameter, and therefore of higher directivity at the same frequency were not great [Fig. 6(a and b)].

In the single focus mode, the performance of arrays consisting of 255 or 256 5-mm elements driven at 1.5 MHz and distributed as square, annular, or hexagonal patterns [Fig. 7(a and c) and Fig. 8] was considerably inferior to that of the 1.5-MHz, 256 5-mm element random array [Fig. 5(b)]. As was mentioned previously, the calculations were carried out with displacements of the focus in both y-z and x-z planes (Fig. 1). For arrays with square [Fig. 3(a and b)] or annular [Fig. 3(c)] patterns, the intensity distributions in the y-z and x-z planes were the same or essentially the same; therefore, in these cases, only the data for the y-z plane were reported here. If the projected views

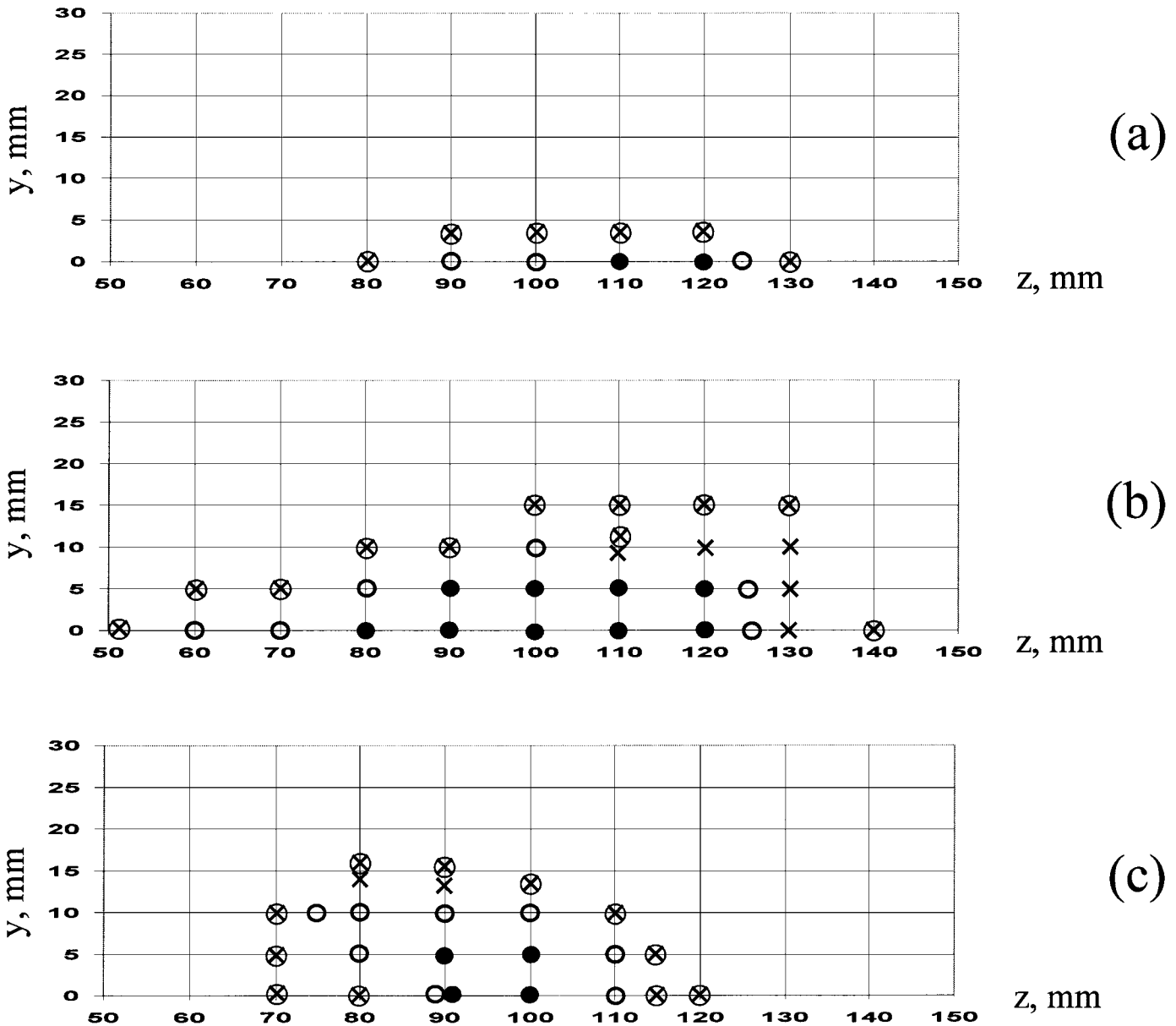


Fig. 7. Assessment of the intensity distributions for the single focus mode associated with regular arrays: a) 256 elements, each 5 mm in diameter, distributed on the shell in a square pattern [Fig. 3(a)]; b) 1024 elements, each 2.5 mm in diameter, distributed on the shell in a square pattern [Fig. 3(b)]; and c) 255 elements, each 5 mm in diameter, distributed on the shell in an annular pattern [Fig. 3(c)]. The frequency is 1.5 MHz. The quality levels are A grade (\bullet), B grade (\circ), C grade (\times), and D grade (\otimes).

of the array structure from location of the focus were different, as in the case of the hexagonal array, the intensity distributions in the y - z and x - z planes were also different [Fig. 8(a and b)]. The best performance among the regular arrays of 255 or 256 elements was that associated with the annular pattern [Fig. 7(c)]; the poorest was that associated with the square pattern [Fig. 7(a)].

The performance of the 1024 2.5-mm element square array [Fig. 7(b)] was considerably inferior to that of the 1.5-MHz, 256 5-mm element random array [Fig. 5(b)] but comparable with the 128 7-mm element random array [Fig. 6(b)]. This implies that randomization of the elements in the array leads, in this case, to a six- to sevenfold decrease in the number of elements (and driving channels)

that maintains approximately the same quality of intensity distribution.

There was a marked difference in the character of the intensity distributions associated with arrays with randomly and regularly distributed elements. In the former only secondary intensity maxima outside the focal area were observed [Fig. 4(a through d)], and grating lobes in the focal plane occurred only in the intensity distributions of very poor quality (data not presented). In the case of regular arrays, relatively high intensities corresponding to grating lobes were observed in the focal plane only.

The results of single focus studies show that if beneficial effects of randomization are to be achieved, then the sparseness of the random array should be within a limited

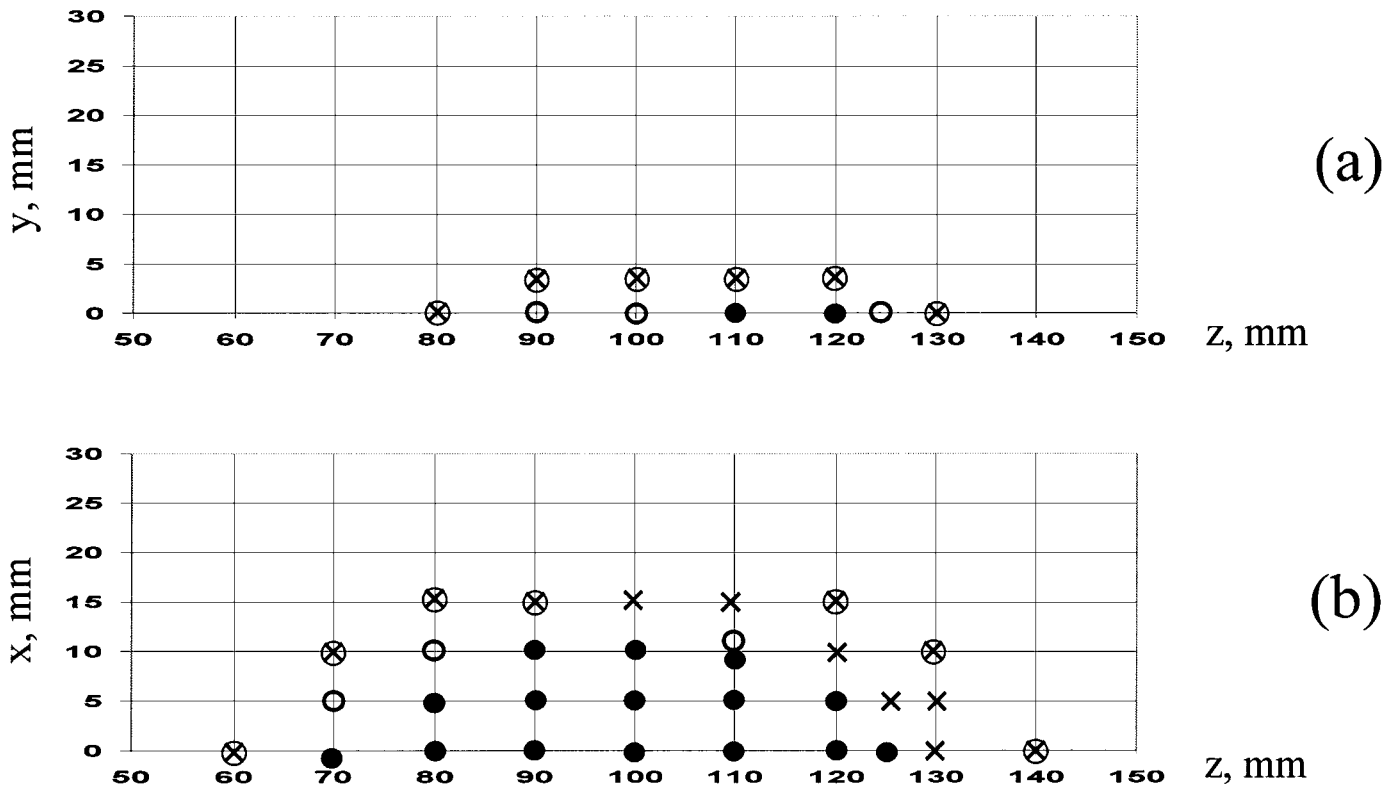


Fig. 8. Assessment of the intensity distributions for the single focus mode associated with regular array of 256 elements, each 5 mm in diameter, distributed on the shell in a hexagonal pattern [Fig. 3(d)]: a) shift of the focus in the y-z plane (Fig. 1) and b) shift of the focus in the x-z plane. The frequency is 1.5 MHz. The quality levels are A grade (●), B grade (○), C grade (×), and D grade (⊗).

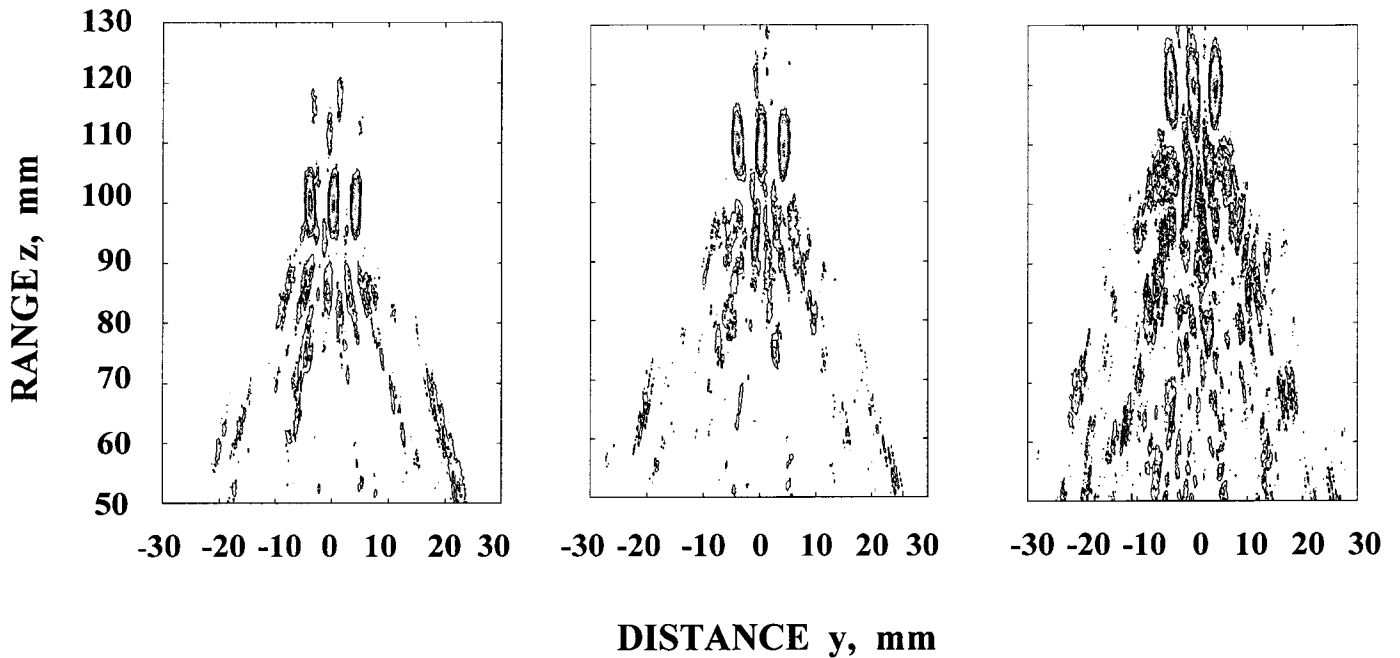


Fig. 9. Classification of intensity distributions associated with generation of simultaneous multiple foci. Left: Grade I ($I \leq 30\% I_{\max}$ outside the focal pattern). Center: Grade II ($30\% I_{\max} < I \leq 40\% I_{\max}$ outside the focal pattern). Right: Grade III ($I > 40\% I_{\max}$ outside the focal pattern). The intensity distributions (in the y-z plane) shown are for the 256×5 -mm element random array with the central focus of the 3×3 coplanar multiple foci pattern at $x = y = 0, z = 100$ mm (left); $x = y = 0, z = 110$ mm (center); $x = y = 0, z = 120$ mm (right).

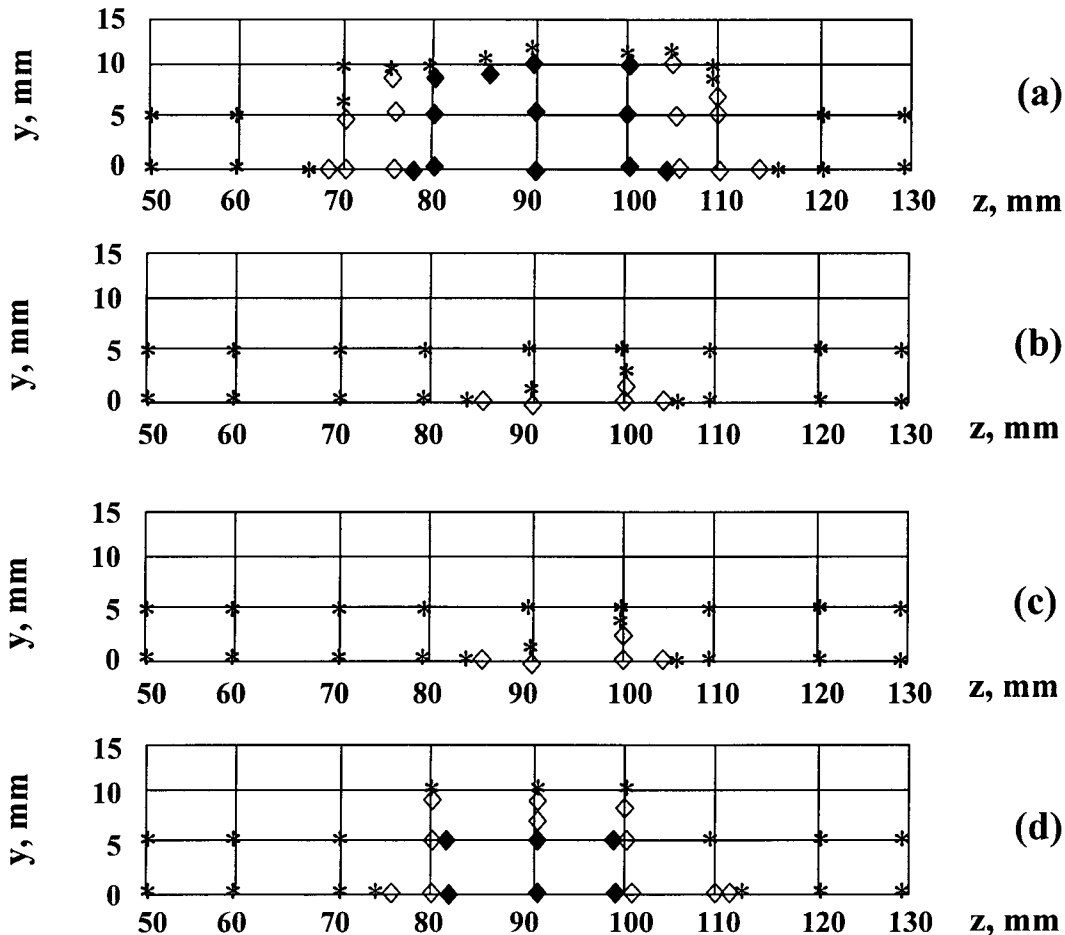


Fig. 10. Summary of results of calculations and quality assessment of the intensity distributions associated with production of simultaneous multiple foci. In each case, nine coplanar foci located on a 3×3 square grid with 4-mm spacing were produced. The coordinates shown refer to those of the central focus in the pattern. a) 256 5-mm diameter elements randomly distributed [Fig. 2(a)]; b) 256 5-mm elements distributed in a square pattern [Fig. 3(a)]; c) 255 5-mm elements distributed in a hexagonal array [Fig. 3(d)]; and d) 255 5-mm elements distributed in an annular pattern [Fig. 3(c)]. In all cases the frequency was 1.5 MHz. The quality levels are grade I (solid diamond), grade II (\diamond) and grade III (*).

range, approximately 40 to 70%. Increasing the level of sparseness results in a decrease of radiated power and deterioration of the quality of the intensity distribution. Decreasing the sparseness leads to an increase in the regularity of the array structure with detrimental consequences.

The performance of the arrays reported here for the single focus mode may be compared with sparse random arrays discussed by Goss *et al.* [11]. They used an array consisting of 108 elements (only 64 of which were activated at any one time), each 8 mm in diameter, driven at a frequency of 2.1 MHz. The elements were mounted in a hexagonal pattern on a section of a spherical shell of diameter 100 mm and radius of curvature 102 mm. The sparseness of the array was approximately 45%. It was shown theoretically that when the array was focused at the geometrical center of the shell, the intensity in the grating lobes in the focal plane was $0.13 I_{\max}$. When the array was focused 5 mm off its central axis, this level was increased to $0.6 I_{\max}$. In experimental measurements, these levels were as high as $0.38 I_{\max}$ and $0.9 I_{\max}$, respectively. Goss *et al.* [11] investigated the effect of randomly locating the

elements on the shell and showed theoretically that the expected level of the intensity in grating lobes in the focal plane would be, in this case, $0.04 I_{\max}$ with no steering and $0.16 I_{\max}$ for steering of ± 5 mm. Such a modest effect of randomization achieved in [11] might be explained by the fact that the ratio of the element diameter to the wavelength was 11.2 in that study. Our results show that a significant effect of randomization could be expected only when the elements are not very directional (element diameter/wavelength ~ 0.5 to 5). Our estimations show that increasing this ratio leads to a significant deterioration of the intensity distributions with the existence of grating lobes.

The results of investigations into the relative performance of 4 1.5-MHz arrays [256 5-mm elements (random pattern), 256 5-mm elements (square pattern), 255 5-mm elements (hexagonal pattern), and 255 5-mm elements (annular pattern)] used to produce a pattern of nine foci, spaced from each other at 4 mm on a square 3×3 grid in a focal plane reflected the general findings of the single focus studies. In the case of the random array, the pattern

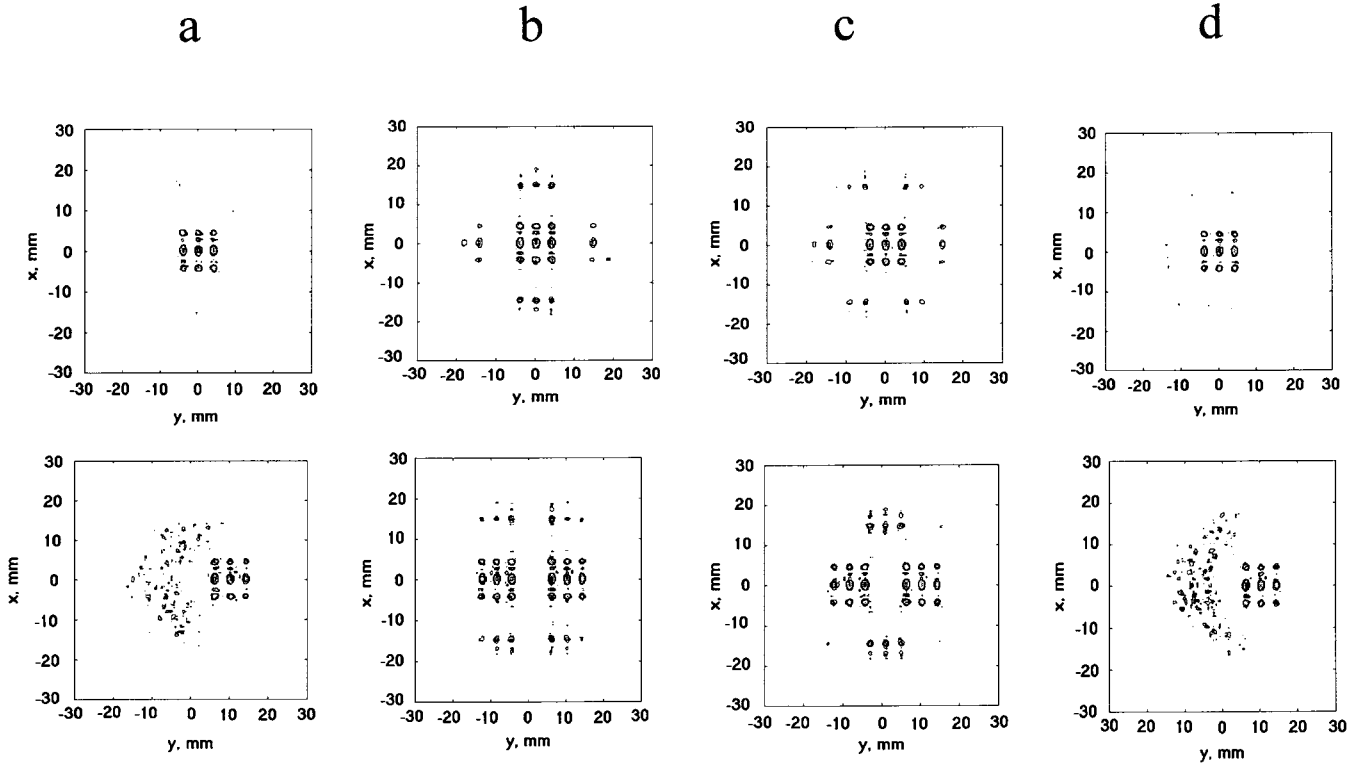


Fig. 11. Intensity distributions calculated in the x - y plane at a range $z = 100$ mm for a 3×3 coplanar pattern of foci separated by 4 mm. The upper graphs are for the central focus in the pattern located at 0, 0, and 100 mm, and the lower graphs are for when it is located at 0, 10, and 100 mm. a) 256 5-mm elements randomly distributed; b) 256 5-mm elements distributed in a square pattern, c) 255 5-mm elements distributed in a hexagonal pattern, and d) 255 5-mm elements distributed in an annular pattern.

of nine foci could be steered along the central axis from 76 to 104 mm and up to 10 mm off the central axis while maintaining a grade I intensity distribution. These distances are with respect to the co-ordinates of the centrally located focus within the 3×3 pattern. The performance was considerably degraded when the elements were distributed in either a square or a hexagonal pattern. In these cases, the best performance was grade II, and this could be achieved only over z values from 86 to 106 mm. With very few exceptions (for example 1 mm off axis at $z = 100$ mm for the square array and up to 2 mm off axis at $z = 100$ mm for the hexagonal array), any steering off the central axis produced a grade III intensity distribution, primarily because of the production of secondary, contra-lateral foci in the focal plane. The 255 elements distributed in the annular pattern achieved intermediate performance with grade I distributions produced when the multiple foci pattern was centered from 81 to 99 mm along the central axis or up to 5 mm off axis. The nature of the problem encountered with the square and hexagonal arrays is highlighted in Fig. 11. The intensity distributions in the focal plane $z = 100$ mm for the cases when the central focus in the 3×3 pattern is either on the central axis or steered off it by 10 mm are both grade III for these arrays [Fig. 11(b and c)]. In the latter case, the intensity values in the grating lobes can be comparable or even higher than in the main lobes. The corresponding intensity distributions for the random and annular arrays [Fig. 11(a and d)] are grade I.

The intensity distributions for multiple foci mode operation were sensitive to the phase values chosen at the foci locations. The phase rotation used here (Table I) was chosen empirically. In another study of phased arrays for ultrasound surgery in which coplanar regular arrays of foci were produced, phases of the complex pressures at the locations of neighboring foci were rotated in other patterns [6], [9]. Improved performance might be achieved if an optimization method is adopted. One method that optimizes the gain has been described [28], but it does not minimize acoustic interference in the near field [9]. The separation between multiple foci of 4 mm used here was not optimized in any way but is comparable with those found to be practical in other studies [6]-[8].

Although the data on multiple-foci presented here only refer to nine coplanar foci placed on a 3×3 grid with spacing of 4 mm, other patterns were considered. Generation of larger patterns such as 5×5 lesions with 2.5-mm separation and 7×7 lesions with 2-mm separation was associated with decreased differences between array performances and a higher frequency of grade III intensity distributions. The f -number (radius of curvature of shell/diameter of array) of the array modeled here was $120 \text{ mm}/110 \text{ mm} = 1.09$ and was slightly greater than those of some other arrays discussed in the literature, which were in the range from 0.8 to 1.02 [7], [8], [11]. Fan and Hynynen [6] have shown that use of an array with a large f -number can exasperate near-field heating, and, therefore, further optimization

of array performance might be achieved by reducing the f-number.

The work presented here is an initial study of the possible advantages for ultrasound surgery offered by random phased arrays. It has highlighted the reduction in grating lobes achievable by degrading the regularity of the locations of the elements on a spherical shell for arrays of similar apertures and effective areas. The results obtained for single foci imply that time-averaged intensity levels associated with scanning of a single focus may be reduced. These general intensity-based advantages appear to be true for a moderate-sized simultaneous multiple foci pattern. More definitive future studies involving the prediction of temperature fields and thermal dose distributions, such as those reported for regular arrays [6]–[8] appear to be warranted. These might address optimization of the number and separation of multiple lesions, the duration of the ultrasound pulses, and the time between them; the f-number and sparseness of the array for particular target sizes and depths will be needed to determine the practical advantages that random arrays may offer. Assessment of the quality of thermal dose distributions, analogous to the assessments of intensity distributions described previously, and referenced to the threshold level for tissue necrosis [8], may prove useful in such studies. Criteria that might be considered are exclusion of thermal doses above the threshold value for tissue necrosis outside of the targeted area or volume for safety reasons, presence of thermal dose values in excess of the threshold value by a moderate factor (e.g., 20-fold as [8]) to reduce the risk of non-necrosis, and exclusion of thermal dose values considerably in excess of the threshold value (e.g., 1000-fold, 10 000-fold, etc.) to avoid unnecessary energy delivery from the array.

V. CONCLUSION

The results of this study suggest that a random distribution of elements on a spherical shell leads to marked improvement of the performance of the array, in terms of the intensity distribution, compared with cases in which regular annular, hexagonal, or square packing is used. As an example, when used to produce a single focus, a random array of diameter 110 mm consisting of 256 circular elements of 5-mm diameter driven at 1 to 1.5 MHz and placed on a spherical shell of the radius of curvature 120 mm was predicted to provide good performance in terms of intensity levels in grating lobes or pre-focal regions. The results obtained for the single focus mode also suggest that comparable performance with a regular array can be achieved while providing a several-fold reduction in the number of elements used. Finally, it was shown that array performance in producing and steering a co-planar square multiple foci pattern, assessed in terms of intensity distributions, is dependent on the degree of order in the array structure. The random array performed better than an array of elements arranged in concentric rings; both performed considerably better than arrays in which the elements were arranged in square or hexagonal patterns,

primarily because of reduced presence of grating lobes in the focal plane.

REFERENCES

- [1] W. J. Fry, W. Mosberg, J. W. Barnard, and F. J. Fry, "Production of focal destructive lesions in the central nervous system with ultrasound," *J. Neurosurgery*, vol. 11, pp. 471–478, 1954.
- [2] F. J. Fry, "Intense focused ultrasound: Its production, effects and utilization," in *Ultrasound: Its Applications in Medicine and Biology, Part II*, F. J. Fry, Ed. New York: Elsevier, 1978, pp. 689–736.
- [3] C. R. Hill and G. R. ter Haar, "Review article: High intensity focused ultrasound—potential for cancer treatment," *Br. J. Radiol.*, vol. 68, no. 811, pp. 1296–1303, 1995.
- [4] H. Rivens, R. L. Clarke, and G. R. ter Haar, "Design of focused ultrasound surgery transducers," *IEEE Trans. Ultrason., Ferroelect., Freq. Contr.*, vol. 43, no. 6, pp. 1023–1031, 1996.
- [5] C. Damianou and K. Hynynen, "Focal spacing and near-field heating during pulsed high temperature ultrasound hyperthermia treatment," *Ultrason. Med. Biol.*, vol. 19, no. 9, pp. 777–787, 1993.
- [6] X. Fan and K. Hynynen, "Ultrasound surgery using multiple sonications—treatment time considerations," *Ultrason. Med. Biol.*, vol. 22, no. 4, pp. 471–482, 1996.
- [7] H. Wan, P. VanBaren, E. S. Ebbini, and C. A. Cain, "Ultrasound surgery: Comparison of strategies using phased array systems," *IEEE Trans. Ultrason., Ferroelect., Freq. Contr.*, vol. 43, no. 6, pp. 1085–1097, 1996.
- [8] D. R. Daum and K. Hynynen, "Thermal dose optimization via temporal switching in ultrasound surgery," *IEEE Trans. Ultrason., Ferroelect., Freq. Contr.*, vol. 45, no. 1, pp. 208–215, 1998.
- [9] X. Fan and K. Hynynen, "A study of various parameters of spherically curved phased arrays for noninvasive ultrasound surgery," *Phys. Med. Biol.*, vol. 41, no. 4, pp. 591–608, 1996.
- [10] T. Fjield, X. Fan, and K. Hynynen, "A parametric study of the concentric-ring transducer design for MRI guided ultrasound surgery," *J. Acoust. Soc. Amer.*, vol. 100, no. 2, pp. 1220–1230, 1996.
- [11] S. A. Goss, L. A. Frizell, J. T. Kouzmanoff, J. M. Barich, and J. M. Yang, "Sparse random ultrasound phased array for focal surgery," *IEEE Trans. Ultrason., Ferroelect., Freq. Contr.*, vol. 43, no. 6, pp. 1111–1121, 1996.
- [12] Y. J. Yoon, P. G. Barthe, and P. J. Benkeser, "Variable-focus lens for ultrasound hyperthermia applications," in *IEEE 1990 Ultrason. Symp. Proc.*, New York, pp. 1661–1664.
- [13] R. J. Lalonde, A. Worthington, and J. W. Hunt, "Field conjugate lenses for ultrasound hyperthermia," *IEEE Trans. Ultrason., Ferroelect., Freq. Contr.*, vol. 40, no. 5, pp. 592–602, 1993.
- [14] T. Fjield, V. Sorrentino, H. Cline, and K. Hynynen, "Design and experimental verification of thin acoustic lenses for the coagulation of large tissue volumes," *Phys. Med. Biol.*, vol. 42, no. 12, pp. 2341–2354, 1997.
- [15] T. Fjield, C. E. Silcox, and K. Hynynen, "Low-profile lenses for ultrasound surgery," *Phys. Med. Biol.*, vol. 44, no. 7, pp. 1803–1813, 1999.
- [16] C. A. Cain and S. I. Umemura, "Concentric-ring and sector-vortex phased-array applicators for ultrasound hyperthermia," *IEEE Trans. Microwave Theory Tech.*, vol. MTT-34, no. 5, pp. 542–551, 1986.
- [17] E. S. Ebbini and C. A. Cain, "A spherical-section ultrasound phased-array applicator for deep localized hyperthermia," *IEEE Trans. Biomed. Eng.*, vol. 38, no. 7, pp. 634–643, 1991.
- [18] S. Umemura and C. A. Cain, "Acoustical evaluation of a prototype sector-vortex phased-array applicator," *IEEE Trans. Ultrason., Ferroelect., Freq. Contr.*, vol. 39, no. 1, pp. 32–38, 1992.
- [19] E. B. Hutchinson, M. T. Buchanan, and K. Hynynen, "Design and optimization of an aperiodic ultrasound phased array for intracavitary prostate thermal therapies," *Med. Phys.*, vol. 23, no. 5, pp. 767–776, 1996.
- [20] E. B. Hutchinson and K. Hynynen, "Intracavitary ultrasound phased array for noninvasive prostate surgery," *IEEE Trans. Ultrason., Ferroelect., Freq. Contr.*, vol. 43, no. 6, pp. 1032–1042, 1996.
- [21] M. I. Skolnik, *Introduction to Radar Systems*. New York: McGraw-Hill, 1980.

- [22] F. Dupenloup, J. Y. Chapelon, D. J. Cathignol, and O. A. Sapozhnikov, "Reduction of the grating lobes of annular arrays used in focused ultrasound surgery," *IEEE Trans. Ultrason., Ferroelect., Freq. Contr.*, vol. 43, no. 6, pp. 991–998, 1996.
- [23] L. R. Gavrilov, J. W. Hand, P. Abel, and C. A. Cain, "A method of reducing grating lobes associated with an ultrasound linear phased array intended for transrectal thermotherapy," *IEEE Trans. Ultrason., Ferroelect., Freq. Contr.*, vol. 44, no. 5, pp. 1010–1017, 1997.
- [24] G. R. Lockwood, P.-C. Li, M. O' Donnell, and F. S. Foster, "Optimizing the radiation pattern of sparse periodic linear arrays," *IEEE Trans. Ultrason., Ferroelect., Freq. Contr.*, vol. 43, no. 1, pp. 7–14, 1996.
- [25] G. R. Lockwood and F. S. Foster, "Optimizing the radiation pattern of sparse periodic two-dimensional arrays," *IEEE Trans. Ultrason., Ferroelect., Freq. Contr.*, vol. 43, no. 1, pp. 15–19, 1996.
- [26] K. Ocheltree and L. Frizzell, "Sound field calculations for rectangular sources," *IEEE Trans. Ultrason., Ferroelect., Freq. Contr.*, vol. 36, no. 2, pp. 242–248, 1989.
- [27] R. J. McGough, M. L. Kessler, E. S. Ebbini, and C. A. Cain, "Treatment planning for hyperthermia with ultrasound phased arrays," *IEEE Trans. Ultrason., Ferroelect., Freq. Contr.*, vol. 43, no. 6, pp. 1074–1084, 1996.
- [28] E. Ebbini and C. A. Cain, "Optimization of the intensity gain of multiple focus phased array heating patterns," *Int. J. Hyperthermia*, vol. 7, no. 6, pp. 951–973, 1991.



Leonid R. Gavrilov was born in Perm, Russia, on May 25, 1938. He graduated from the Leningrad (now St. Petersburg) Electrotechnical Institute, Department of Electronic Engineering, in 1961. He received the Ph.D. in engineering for a dissertation related to the development of methods of measurements distributions of the size and number of gas bubbles-cavitation nuclei in liquids from the Central Institute of Turbo-Machines, Leningrad, in 1966. He also received the D.Sc. degree from the N. N. Andreev Acoustics Institute, Moscow, for his dissertation, "Investigations of the effects of focused ultrasound on biological structures for application in medicine and physiology" in 1982.

Since 1967, he was with the N. N. Andreev Acoustical Institute, Moscow, studying initially the acoustical properties of gas bubbles in liquids and, since 1969, the application of focused ultrasound in medicine and physiology. Since 1980, he has been Head of the Laboratory of Medical Acoustics in this institute. From 1993 to 1994, he was an Honorary Senior Research Fellow in the Queen's University of Belfast, UK, and, from 1995 to 1998, he was a Senior Research Officer in the Radiological Sciences Unit, Hammersmith Hospital, London. His current research interests are in the application of focused ultrasound for stimulation of neural structures, in therapeutic application of ultrasound (in particular, in the development of phased arrays for surgery and ultrasound hyperthermia), and in biological effects and safety aspects of ultrasound.

Jeffrey W. Hand was born in Alvaston, Derby, England on June 13, 1946. He obtained the B.Sc. (Hons Physics) degree in 1967 and the Ph.D. degree for his dissertation, "Cyclotron resonance of free electrons," in 1972. Both were awarded by the Faculty of Science, University of Newcastle-upon-Tyne. In 1995, he received the D.Sc. degree from the Faculty of Medicine, University of Newcastle-upon-Tyne for his dissertation, "Physical techniques and their application for hyperthermic therapy."

From 1976 to 1992, Dr. Hand developed microwave, RF, and ultrasound heating techniques; thermometry; and quality assurance criteria for clinical hyperthermia at the UK Medical Research Council's Cyclotron Unit at Hammersmith Hospital, London. From 1992 to 1994, he was Head of Health & Diagnostic Physics within the Department of Medical Physics, Hammersmith Hospital. He is currently Director of the Radiological Sciences Unit, Imaging Directorate, Hammersmith Hospital, and is Reader in Imaging Physics in the Department of Imaging, Imperial College School of Medicine (Hammersmith Campus), London. He has held several temporary posts including Research Professor at the University of Arizona, Visiting Scholar at Stanford University, and a Fellowship of the Japan Society for the Promotion of Science Fellowship at Shimane Medical School, Izumo, Japan.

His current research interests include the therapeutic uses of ultrasound fields, electromagnetic modeling, safety aspects of magnetic resonance imaging and spectroscopy, and applications of microwave radiometry in neonatal medicine. Dr. Hand is a Fellow of the Institute of Physics, a Fellow of the Institution of Electrical Engineers, and a Fellow of the Institute of Physics and Engineering in Medicine. He was Chair of the IPEM Ultrasound and Non-Ionizing Radiation Special Interest Group in 1998 to 1999 and is currently a member of the IPEM Engineering Group Board.

His current research interests include the therapeutic uses of ultrasound fields, electromagnetic modeling, safety aspects of magnetic resonance imaging and spectroscopy, and applications of microwave radiometry in neonatal medicine. Dr. Hand is a Fellow of the Institute of Physics, a Fellow of the Institution of Electrical Engineers, and a Fellow of the Institute of Physics and Engineering in Medicine. He was Chair of the IPEM Ultrasound and Non-Ionizing Radiation Special Interest Group in 1998 to 1999 and is currently a member of the IPEM Engineering Group Board.